

# AUV5500: Advanced in-situ dry cleaning and metrology process for next generation lithography

Christian Chovino, Stefan Helbig\*, Peter Dress\*

Dupont Photomask Assignee, New Technologies, Advanced Mask Technology Center (AMTC) GmbH & Co. KG  
Rähnitzer Allee 9, 01109 Dresden, Germany

\*Advanced Process Division, STEAG HamaTech AG, Ferdinand-von-Steinbeis-Ring 10, 75447 Sternefeld, Germany

## ABSTRACT

Today, the industry is suffering from the consequences of residue and contaminants on the mask surface as they significantly affect the printing quality of the reticle. As the industry is moving forward toward smaller feature sizes with the next generation lithography (NGL), i.e. 193nm immersion and EUV, it is more than likely that effect of contaminant will worsen. Thus a good control of the mask cleanliness via its optical properties is becoming essential to minimize the impact of contaminants while achieving the tight specification of mask customers for NGL.

The AUV5500 is specifically addressing contaminants. The principle of the tool set-up, its process functionality is presented. The first process results on binary and PSM masks are analyzed and discussed.

**Keywords:** dry cleaning, inspection, NGL, photomask, organic contamination

## 1. INTRODUCTION

Mask cleaning has always been a challenge for the semi-conductor industry mainly because of the mask material susceptibility to the chemistry applied. Nonetheless, the industry was able to successfully develop wet cleans based on sulfuric and ammonia chemistry with good cleaning efficiencies and minimum impact on the mask optical properties. The purpose of the sulfuric is the removal of organics whereas the ammonia mainly addresses the particles as it removes the top layer of the film. As the industry is moving forward toward smaller nodes and new mask materials are being investigated for the Next Generation Lithography, i.e. EUV, the traditional cleans are showing limitations in their capabilities to provide the level of cleanliness required for the future nodes without damaging the mask material. Furthermore, in the case of EUV technology, it is known that organic residuals are to be removed from the mask, as they significantly alter the optical properties of the same, resulting in some cases up to 22% of reflectivity loss at the wavelength of use [1].

In addition, for the last couple years, the industry has been struggling with crystal growth and haze formation on mask surface [2]. The crystal growth impacts the wafer fab as it results in printing defects and ultimately yield loss. It is believed from various studies that the mask residues from the wet cleans, are in part responsible for the growth [3,4]. Although, new processes are being developed to minimize haze issue [5,6], the need for alternative cleans is pressing and it becomes a necessity to investigate sulfate free cleans. Through this paper we are investigating a dry cleaning tool based on Ultra-Violet (UV) exposure at 172nm in conjunction with an adjustable environment as a mean to remove organics residuals. Although the capability of UV for organic removal agent has been demonstrated and is not new in essence, the novelty presented here resides in the in-situ capability from the integration of the UV unit with a spectrometer capable of reflectivity and transmission measurement in the Deep UV where organic thin films are optically sensitive. Therefore it is conceivable to envision a process where the spectrometer would acknowledge the cleaning status with regard to film contaminants via transmission and reflection measurements at a wavelength of choice throughout the complete reticle.

To achieve this functionality, it is necessary to first distinguish between the optical effects from the surface contaminants on one hand and the structures on the other hand. In this paper, we are beginning this study by presenting the tool functionality, the first results of contaminants effect on bare surfaces and the optical responses of simple structures.

## 2. AUV5500: TOOL CONCEPT

The emphasis of the AUV 5500 is the ability to remove organic residuals and contaminants of the mask surface (6" x 6"), of concern to the industry, and to verify in-situ the result of the cleaning by measuring the transmission and the reflection. The combination of the dry UV-cleaner with a spectrometer unit provides a good control of the cleaning process that minimizes a possible alteration of the mask optical properties.

### 2.1. General process stations and the related process functions

The AUV5500 tool comprises four stations, as illustrated on the sketch of the tool layout on Figure 1. A SMIF (Standard Mechanical Interface) unit serves as a defined interfacing between the AUV5500 tool and any other process tool part of the mask manufacturing process. A robot automatically handles the mask inside the tool. The process flow is defined via the Graphical User Interface (GUI). A flip station offers the opportunity to clean and investigate both surfaces of the reticle. The two main stations of the tool are the UV station to remove organic layers from the mask surface and the spectrometer station that acknowledges the reticle surfaces cleanliness before and/or after a cleaning process. Both stations are described in more detail in the following sections. The air inside the tool is re-circulated within a close loop that contains chemical and particle units combined with a temperature control system. The filtration assembly provides a class 1 or better clean room environment with amine levels <1ppb, and TOC- (Total Organic Compounds) concentration <5ppb in the path of the mask during all handling operations inside the tool.

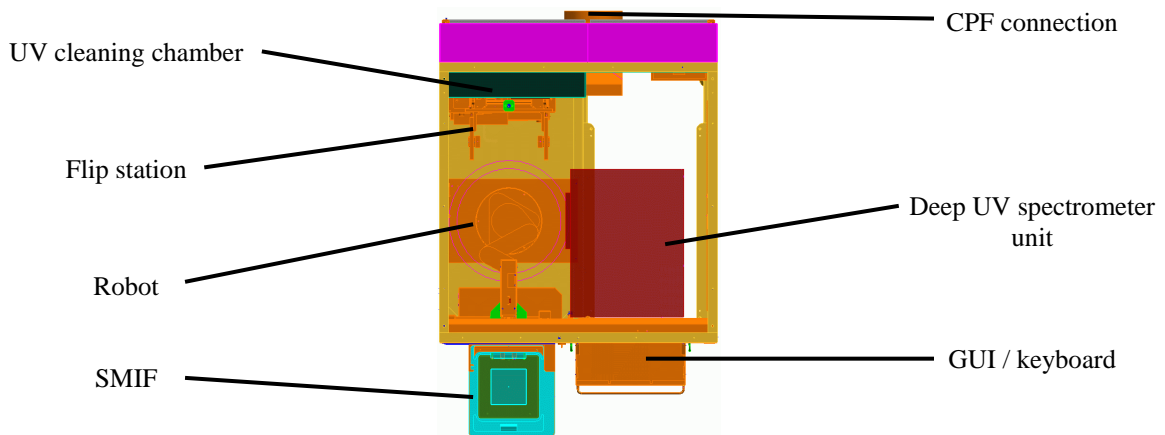


**Figure 1:** Sketch of the AUV 5500 layout illustrating the tool principle together with the process stations.

### 2.2. Deep UV spectrometer unit

The deep UV spectrometer unit comprises of a sample chamber and a UV spectrometer. The UV spectrometer is operating in the spectral range of 145nm to 270nm. It relies on a blazed reflection grating as dispersion unit and uses a deuterium lamp as the light source. A spectral resolution of 0.71nm in combination with an absolute wavelength accuracy of  $\pm 0.08\text{nm}$ , is determined by utilizing the atomic emission line at  $\lambda=121.5339\text{nm}$  [7] of a deuterium light source throughout the complete spectral range. Three different photo-multiplier tubes (PMT) are used to measure simultaneously transmitted, reflected and light source intensity (see Figure 2). Absolute transmission and reflection are calculated from referencing these measurements to the data determined on a standard sample. The reflection standard is well known and optically characterized. It sits in a chuck next to the mask (see Figure 3). A hole in the chuck serves as transmission standard (see Figure 3).

The spectrometer chamber includes the mask chuck onto a (x,y)-table enabling the scanning of the mask surface. Thus, the mask is moved to the locations of choice; within the optical path. It is held "face-down". The light spot size is 800 $\mu\text{m}$  in diameter throughout the complete optical range.

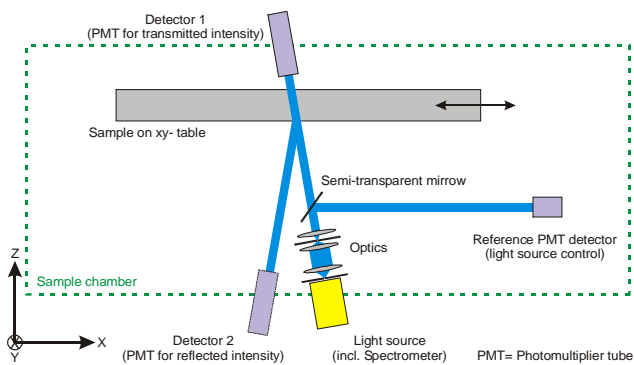


**Figure 2:** Schematic principle of the optical set-up inside the spectrometer chamber measuring the transmitted and reflected intensity

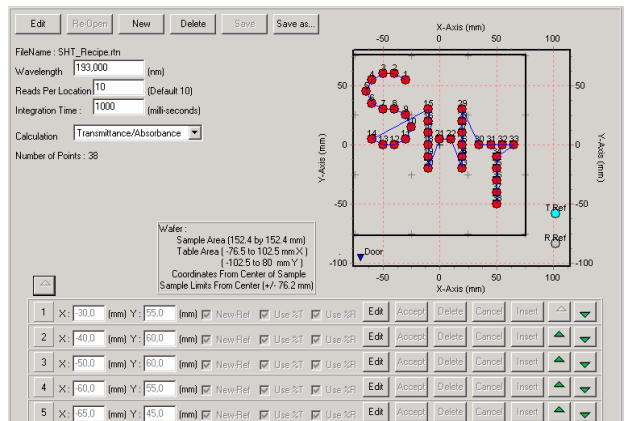


**Figure 3:** Screen shot of the GUI editor used to define a grid on the reticle surface; with some of the spectrometer parameters, e.g. integration time, wavelength of interest.

Figure 3 represents a view of the GUI defining the measurement process by specifying the measurements locations, the wavelength of choice, the integration time per reading and the number of readings per location. A continuous flushing of the entire UV spectrometer unit is performed with ultra- pure nitrogen (99.9999%) to eliminate any optical influence on the readings from oxygen or other gas susceptible to interfere in this optical range. Temperature and humidity inside the spectrometer unit are continuously monitored within  $\pm 0.1^\circ\text{C}$  and  $\pm 0.1\%$  respectively, to ensure stable measurement conditions.

### 2.3. UV cleaning chamber (172nm)

The dry-cleaning process of the mask surface is performed in the UV cleaning chamber by illuminating the surface with 172nm light (excimer lamp). In addition, a defined gas mixture can be introduced to the process chamber predominantly filling the gap between the mask surface and the exit window of the illumination light source. Current gases include nitrogen dry and wet, argon (dry) and oxygen (dry). The gases flows are controlled accurately to provide levels down to ppms of active constituents. Figure 4 illustrates the principle design of the media supply system. Each contributing gas volume is controlled by a mass flow controller (MFC), and then is mixed with the other species inside a separated mixing labyrinth before entering the process chamber. The editor in the GUI enters the flow volumes into more 'conventional' units, e.g. vol.% and/or ppm (See shaded gray on Figure 5).

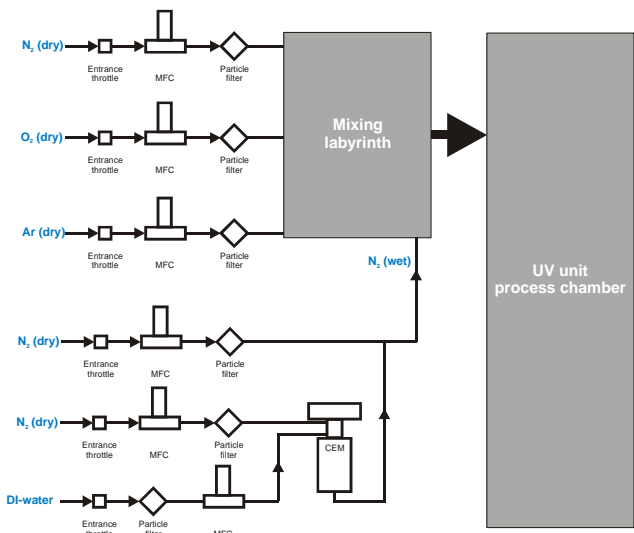


**Figure 4:** Media layout illustrating the design principle of the media supply system to the UV cleaning chamber.

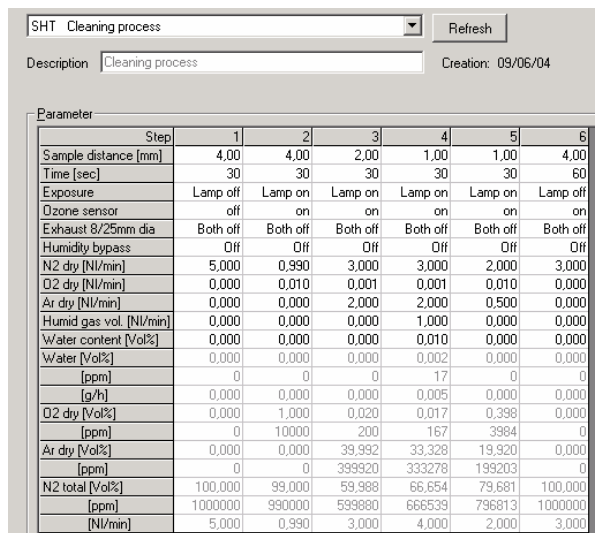


**Figure 5:** Typical screen shot of the GUI editor defining the cleaning process in the UV cleaning chamber.

The gap between the sample and UV light source is adjustable as parameter of the process. A typical cleaning program consists of several steps (columns, on Figure 5), with its own time period and process conditions. Given the right process conditions, combining oxygen with 172nm UV light will result in the formation of ozone and atomic oxygen. Both species are known to be active contributors to the cleaning efficiency of the process [8-10].

### 3. PROCESS PERFORMANCE

#### 3.1. AUV5500 system characterization

Since this tool is a prototype, the first series of measurement were targeting the repeatability. The absolute reflectivity is measured at four wavelengths on a binary mask blank, on a 3x3 array covering a field of 100mm x 100mm .The measurements wavelengths chosen were  $\lambda=157\text{nm}$ , 193nm, 248nm, and 257nm. The same array was repeatedly measured ten times without interruption from loading and/or unloading of the blank in the spectrometer. The integration period for the data reading was set to 1second. Figure 6 illustrates the data collected at a measurement wavelength of 193nm for all nine different locations. Although we are beginning with different reflectivity, the repeatability of the readings is clearly demonstrated for all investigated wavelengths. The standard deviation corresponding to a 99.8% confidence level ( $3\sigma$ ) is summarized in table 1 for each wavelength. Wavelengths larger than 193nm showed lower  $3\sigma$  0.03%, whereas 157nm wavelength shows the larger  $3\sigma$ -value, 0.093%. This result might originate from to the higher sensitivity of the intensity readings to the gas atmosphere inside the spectrometer unit (spectrometer and sample chamber). Figure 7 illustrates the dispersion of the absolute reflectivity of the binary blank in the spectral range from 157nm to 257nm.

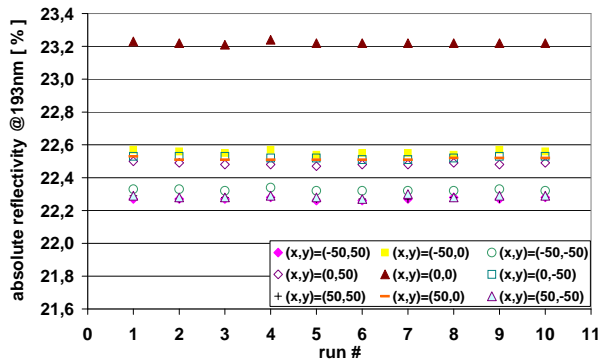


**Figure 6:** One example of the repeatability test results (absolute reflectivity at 193nm) for nine different locations covering a central area on a binary blank.

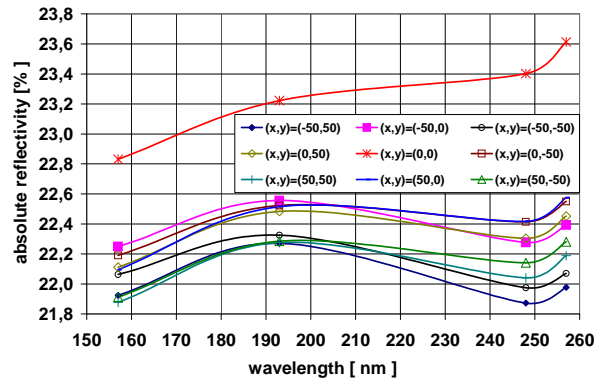


**Figure 7:** Dispersion graphs for the absolute reflectivity (mean value of the ten readings at each location) of a binary blank surface at nine different locations.

	Measurement wavelength			
	157nm	193nm	248nm	257nm
$3\sigma$	0.093%	0.024%	0.018%	0.018%

**Table 1:** Repeatability results at four characteristic lithographic wavelengths. The data shown are the absolute standard variation values of repeated measurements with an integration period of 1s.

#### 3.2. First cleaning results

A controlled contamination process was developed to study the cleaning capability of the tool. The contaminant of choice was isopropyl alcohol. The cleaning efficiency was evaluated by measuring the reflectivity of the blank at 157nm, 193nm and 257nm. Figure 8 represents as an example the reflectivity measured at 157nm and 193nm at 5 locations. The blank was cleaned prior to contamination: A series of measurement was collected after each step:

- Before contamination: Pre measurement
- After contamination: Post contamination
- After UV clean: Post UV cleaning

### 3.2.1. Mask Blanks

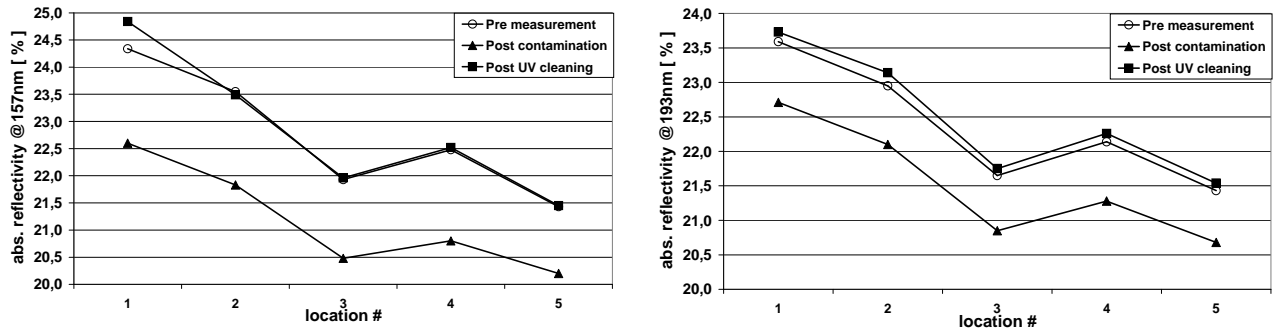


**Figure 8:** Absolute reflectivity from five locations on a binary blank, before and after the contamination with IPA and after dry UV clean. The left graph illustrates the results at 157nm and the right graph at 193nm inspection wavelength.

A consistent drop of the reflectivity is noticeable after contamination. The drop represents 1,8% and 1% at 157nm and 193nm respectively. The effect of the contaminant is more severe at 157 than at 193nm. This is no surprise, since organic contaminants were identified as one of the concerns during the development of the 157nm Lithography [11]. After cleaning, the reflectivity is recovered at each location. The 193nm reflectivity data reveals 99.5% recovery of the initial reflectivity at 193nm. Further investigation reveals a time dependant effect associated with the gap of the reflectivity. After the UV clean, the surface is active and will inherently grow organic resulting in a slight drop of the reflectivity to reach a steady value. It is not exactly understood at this stage why this phenomena is more pronounce at 193 than 157nm. We are suspecting the nature of the contaminant as a possible route cause.

### 3.2.2. Binary Reticles

A scanning protocol was developed to investigate the impact of adjacent surfaces and standard type features on the transmission and reflection measured with the spectrometer. On Figure 9, we describe the scanning from a chrome surface to a quartz surface. The circle represents the measurement spot. The scanning is performed in increments of 100 $\mu$ m starting on the chrome and heading onto the quartz surface.

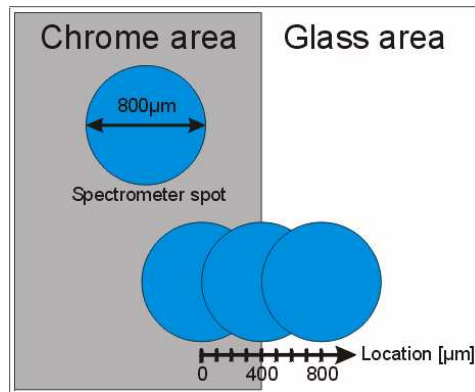


**Figure 9:** Illustration of the spectrometer spot scanning across the edge of adjacent chrome and quartz surfaces

Both transmission and reflection curves show a step-type function from one surface to the other, as represented on Figure 10. The reflection curve exhibits a linear portion from the quartz surface to the chrome surface. Indeed, scanning from the chrome to the quartz surface, the amount of light going through the quartz is continuously increasing. This increase is directly depending upon the amount of clear field within the measurement spot. This behavior indicates the absence of interferences between the reflective lights off the respective surfaces. Because of the significant difference between the optical properties ( $n$ ,  $k$ ) of the respective surfaces interferences are not likely to occur in the wavelength range of study.

In a first approximation, the values for the reflection were derived from the reflection of the single surface (quartz, MoSi) by considering the ratio  $D$  of the feature size area ( $A_{Feature}$ ) to the spectrometer spot area ( $A_{Spot}$ ).

Thus, the reflectivity on the feature is given by:  $R_{Feature}: R_{Feature} = D * R_{Quartz} + (1 - D) * R_{Chrome}$  (1)

A verification of this calculation is provided on Table 2 where we compare calculated and experimental data.

Interestingly the transmission shows the same trend. A linear relationship is noticeable as well. A similar equation for the transmission of the feature  $T_{Feature}$  was derived:  $T_{Feature} = D * T_{Quartz} + (1 - D) * T_{Chrome}$  (2)

In this particular case, the equation is simplified since the chrome does not transmit at all in the wavelength range. Thus equation 2 becomes:  $T_{Feature} = D * T_{Quartz}$  (3)

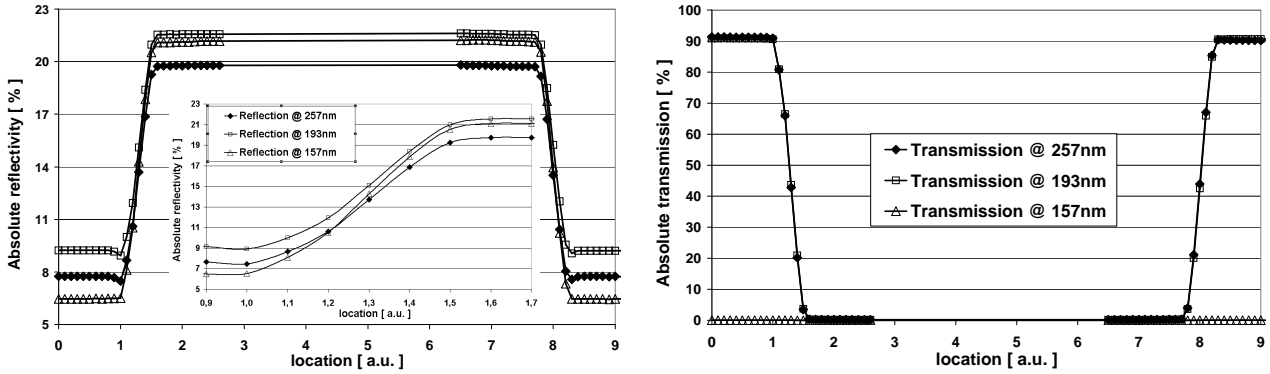


**Figure 10:** Measurement of the absolute reflectivity (left graph) and transmission (right graph) values with the spectrometer measurement spot scanning across a chrome area (two chrome/quartz edges). The graphs show the results for the three wavelengths of 157nm, 193nm and 257nm before the IPA contamination.

Location (a.u.)	Transmission (%)		Reflection (%)	
	Measured	Calculated	Measured	Calculated
1.1				
1.2				
1.3				
1.4				
1.5				

**Table 2:** Comparison of calculated and experimentally measured transmission and reflection at 193nm in the linear portion of the scanning process.

A closer analysis of the variation of the curves with the wavelength exhibits a change in the slope of the reflectivity throughout the scan. Table 3 shows the mean slopes values calculated from R and T at different locations for each wavelength. The change in slope with wavelength is mainly attributed to the material optical properties varying throughout the spectrum.

	Mean slope @257nm		Mean slope @193nm		Mean slope @157nm	
	Reflectance	Transmission	Reflectance	Transmission	Reflectance	Transmission
<b>PRE</b>	26.67	187.33	26.69	186.59	32.39	0.11
<b>CONT</b>	24.77	184.64	25.88	185.34	30.41	0.12
<b>POST UV</b>	27.48	187.03	27.42	186.63	33.64	0.10

**Table 3:** Comparison of the mean slopes collected from a series of scans across adjacent surfaces at the different wavelengths in transmission and reflection mode. The values are reported before contamination (PRE), after contamination (CONT) and after the UV cleaning (POST UV).

The linear behavior was still noticeable with the addition of the contaminant. A decrease of the slope is visible for every wavelength. As we explained before, the absolute reflectivity is dropping with the addition of the contaminant, thereby decreasing the slope of the reflectivity /transmission with the scanning position. The contaminant is acting as a buffer layer that reduces the effect of each single layer by averaging the optical properties of each surface (chrome and quartz). It is conceivable to envision an increase of this effect, slope reduction, with the thickness of the film of contaminant film to a certain extent.

### 3.2.3. PSM Reticles

The impact of the UV clean process on 193nm phase shift material was evaluated as well. The mask design was consisting of 9 phase cells distributed in a 3x3 array throughout the mask active field. The phase and transmission measurements were collected on an MPM 193 from Lasertec. The phase and transmission change representative of the difference of the mask properties before and after clean are presented on Figure 11. Both phase and transmission show minimal variations well in the range of the tool accuracy:  $\pm 0.4^\circ$  in phase and  $\pm 0.1\%$  in transmission respectively. One can conclude that the UV clean process does not affect the optical properties of the reticle.

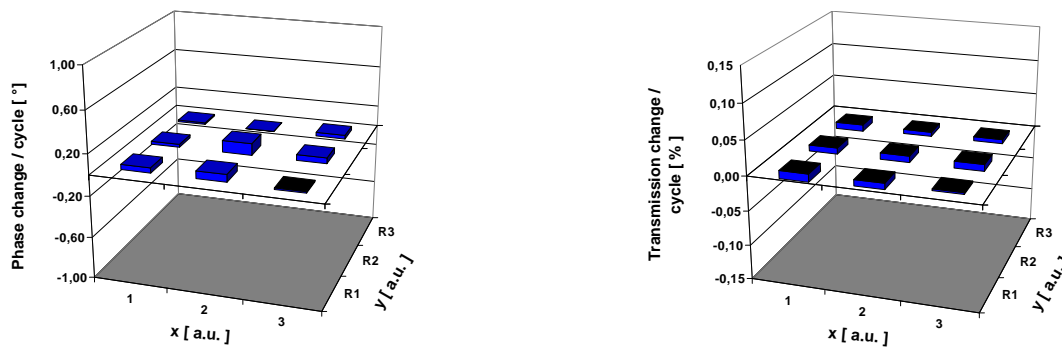


**Figure 11:** Change of the phase (left graph) and the transmission (right graph) properties across the PSM reticle surface per IPA contamination & UV clean process.

#### 3.2.3.1. Measurement on standard features

The same matrix, described above was used for the measurements on standard structures. Reflection and transmission readings were performed at five wavelengths, namely, 147nm, 157nm, 193nm, 257nm and 270nm. The phase cells were used as standard features. The spot was centered on the feature, covering it completely for each measurement (Refer to the illustration in Figure 12).

The design contains open fields enabling measurements on MoSi or Quartz only. The transmission and reflection measurements are reported on Table 4. The first two columns represent the experimental data whereas the last two are calculated from Equations 1 and 2 described above.

$\lambda$	Measurement		Model calculation	
	Reflectance [%]	Transmission [%]	Reflectance [%]	Transmission [%]
147nm	47.93	0.08	47.08	0.08
157nm	19.35	0.01	19.32	0.01
193nm	17.88	14.52	18.29	15.74
257nm	14.58	34.99	14.91	35.44
270nm	14.20	39.05	14.57	39.30

**Table 4:** Comparison of the calculated and measured reflectivity and transmission at different wavelengths of quartz on MoSi surface.

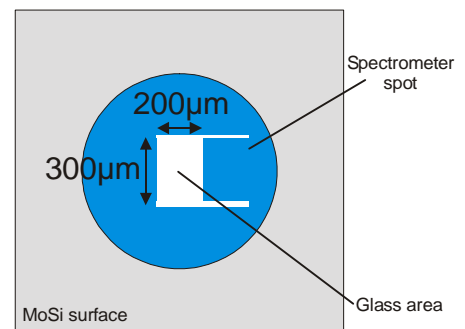


**Figure 12:** Illustration of the spot position on a standard feature.

The calculation emphasizes a good correlation between measured and calculated values. The differences observed are assumed to originate from the Gaussian intensity profile of the spectrometer spot, not considered in the calculation. In addition, it is understandable that this first approximate theoretical approach remains valid only if the structures investigated are much greater ( $10 \lambda$ ) than the measurement wavelength.

### 3.2.3.2. Measurement on typical structures

Transmission and reflection were measured on  $6\mu\text{m}$  pitch lines and spaces pattern of 1:1 duty cycle from 147nm to 270nm. The results are reported on Figure12.

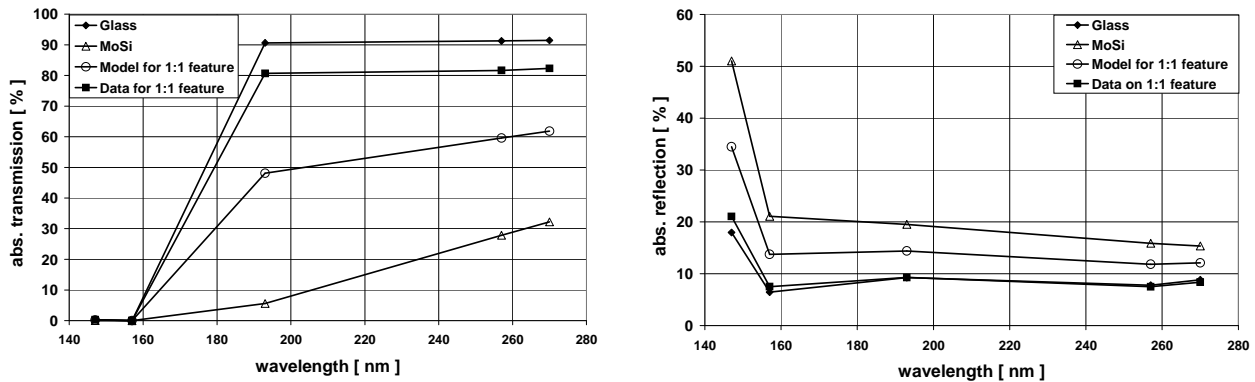


**Figure 12:** Dispersion of the transmission and reflection of MoSi and quartz in the spectral range from 147nm to 270nm. In comparison transmission and reflection data measured on the real feature and the graph according to the simple theoretical approach are included.

Both reflectivity and transmission are confined in the region delimited by the single surface data. The first order equation defined for the standard structures does no longer represent the results for this type of features, as one can see Figure 12. The lines and space features generate diffraction orders modifying the intensity of the light detected. Thus, a more sophisticated model is required to replicate this behavior. It will be the subject of a future paper.

## 4. CONCLUSION

In this paper we presented the principle and the functionality of the AUV 5500. The first results on controlled organic contamination on binary and PSM reticles were presented as well. The contaminant is altering the mask optical properties via a decrease in reflectivity in the Deep UV. We demonstrated the ability to efficiently remove the contaminant via a UV base process without altering the reticle optical characteristics. The optical response of simple features was investigated. A first order equation based on a linear relationship with the optical characteristics of the individual respective surfaces was proven to accurately reproduce the experimental optical response of the simple structures. It justifies the purpose of this tool; assess both the presence and the cleaned-off of a contaminant on a structure.

## ACKNOWLEDGEMENT

Dr. P. Dress and S. Helbig thank Bob Jarratt, Paulo Goulart, Bob Fancy, and Chuck Lowe from Acton Research Corp., U.S.A. for their technical support and the fruitful discussions during the spectrometer set-up period. Part of this work is performed under financial support of BMBF (Bundesministerium für Bildung und Forschung) as part of the project “Abbildungsmethodiken für nano- elektronische Bauelemente” (FKZ 01M3154H).

## REFERENCES

- [ 1 ]: A. Barty, K. A. Goldberg, “The effects of irradiation induced contamination on the performance of an EUV lithographic optic”, *SPIE Proceedings* **5037**, 2003, p. 450-459
- [ 2 ]: E.V. Johnstone, L. Dieu, C. Chovino, J. Reyes, D. Hong, P. Krishnan, D. Coburn, C. Capella, “193nm Haze Contamination: A close Relationship between Mask and its Environment”, 23<sup>rd</sup> Annual BACUS Symposium on

- Photomask Technology, *SPIE Proceedings* **5256**, 2003, p. 440-448.
- [ 3 ]: F. Eschbach, D. Selassie, P. Sanchez, D. Tanzil, V. Tolani, M. Toofan, H. Liu, B. Greenebaum, M. Murray, R. Villacorta, "ArF lithography reticle crystal growth contributing factors", 24<sup>th</sup> Annual BACUS Symposium on Photomask Technology, *SPIE Proceedings* **5567**, 2004, p. 497-505.
  - [ 4 ]: B.J. Grenon, C. Peters, K. Battacharyya, W. Volk, "Formation and Detection of Sub-pellicle Defects by Exposure to DUV Illumination", 19<sup>th</sup> Annual BACUS Symposium on Photomask technology, *SPIE Proceedings* **3873**, 1999, p. 162-176.
  - [ 5 ]: F. Eschbach, D. Tanzil, M. Kovalchick, U. Dietze, M. Liu, F. Xu: "Improving photomask surface properties through a combination of dry and wet cleaning steps" in *Photomask and Next-Generation Lithography Mask Technology XI* (Hiroyoshi Tanabe) *SPIE Proceeding* **5446**, 2004, p. 209-217
  - [ 6 ]: E.V. Johnstone, C. Chovino, J. Reyes, L. Dieu: "Haze control: Reticle/environment interactions at 193nm", *Solid State Technology*, May 2004, p. 69-73
  - [ 7 ]: R.L. Kelly, L.J. Palumbo: "Atomic and ionic emission lines below 2000 Angstroms – hydrogen through Krypton" (NRL report #7599), p. 4, Naval Research Laboratory, Washington, June 1973
  - [ 8 ]: Z. Falkenstein, J.J. Coogen: "Photoresist etching with dielectric barrier discharges in oxygen", *J. Appl. Phys.* **82**, Nr.12, 15. Dec. 1997, p. 6273-6280
  - [ 9 ]: Z. Falkenstein: "Effects of the O<sub>2</sub> concentration on the removal efficiency of volatile organic compounds with dielectric barrier discharges in Ar and N<sub>2</sub>", *J. Appl. Phys.* **85**, Nr.1, 01. Jan. 1999, p. 525-529
  - [ 10 ]: Z. Falkenstein: "Ozone formation with (V)UV-enhanced dielectric barrier discharge in dry and humid gas mixtures of O<sub>2</sub>, N<sub>2</sub>/O<sub>2</sub>, and Ar/O<sub>2</sub>", *Ozone Science & Engineering* **21**, 1999, p. 583-603
  - [ 11 ]: C.M. Schilz, K. Eisner, S. Hien, T. Schleussner, R. Ludwig, A. Semmler: „Influence of e-beam induced contamination on the printability of resist structures at 157nm exposure", *SPIE Proceeding* **4562**, 2001, p. 297-306